Commercial and recycled carbon/steel fibers for fiber-reinforced cement mortars with high electrical conductivity

(Article begins on next page)

Commercial and recycled carbon/steel fibers for fiber-reinforced cement mortars with high electrical conductivity

Alberto Belli[1], Alessandra Mobili[1], Tiziano Bellezze[1], Francesca Tittarelli[1,2]

[1]*Department of Materials, Environmental Sciences and Urban Planning (SIMAU), Università Politecnica delle Marche, Via Brecce Bianche 12, 60131, Ancona, Italy – INSTM Research Unit.*

[2]*ISAC – CNR, Via Piero Gobetti 101, 40129, Bologna, Italy.*

Corresponding author: Tel. +39 071 2204732.
E-mail address: f.tittarelli@univpm.it (F. Tittarelli).

Abstract

The paper aims to provide a comprehensive study on the compositional optimization of high-conductive multifunctional fiber-reinforced cement mortars (FRCMs). Therefore, the effects of three different fiber types: virgin carbon fibers (VCFs), recycled carbon fibers (RCFs), and brass-plated steel fibers (BSFs), added at a broad range of concentrations, as 0.05%, 0.1%, 0.2%, 0.4%, 0.8%, 1.2%, and 1.6% by volume, on the mechanical, electrical and durability properties of FRCMs have been compared. The results showed that RCFs increase the flexural and tensile splitting strength up to 100%, whereas BSFs improve the compressive strength by 38%. Moreover, the fibers decrease both the capillary water absorption and the drying shrinkage by 39%. Electrical conductivity tests show that RCFs decrease the electrical resistivity of mortars up to one order of magnitude, in addition to a percolation threshold between 0.1 and 0.2 vol.%.

1. Introduction

Concrete is the most commonly used material in the construction industry [1], and it remains as the basic component that characterizes modern building techniques. Recent discoveries in material engineering have allowed concrete technology to evolve, thereby improving its traditional structural properties and integrating hardened composites with new functions through the incorporation of innovative and high-performance materials [2].

In recent decades, research has been increasingly focused on processes to reduce the carbon footprint of ordinary Portland cement (OPC), which accounts around 8% of global CO_2 emissions [3,4], by using recycled industrial by-products and enhancing the resistance and durability of cement-based composites, in order to decrease the resource supply and strive for a more sustainable construction industry [5]. In addition, in recent years, an increasing number of properties are required from building materials, due to the growing social interest in structural safety and to improve the quality of life within buildings [6–10].

The addition of electrically conductive fibers into the cement-based materials both improves the mechanical performance and durability of the composites [11] and enlarges their functionality by improving their electrical properties [12–14].

Highly conductive mortars and concretes could be used for structural health monitoring (SHM) systems, by producing piezoresistive cement-based strain-sensors (PCSSs) [15,16] and self-heating and defrosting surfaces (to avoid the use of thawing salts, which are harmful to reinforced concrete) [17]. These additional functions could enhance the structures' safety and the life cycle of the building products, thereby decreasing the resources necessary for their maintenance. Moreover, highly conductive cementitious materials could be used as sensors for traffic monitoring [18], as energy collectors [7,19], and for electromagnetic interference (EMI) shielding [20].

Many authors have experimented with different types of admixtures for the reinforcement of mortar and concrete, and to improve their electrical properties. In particular, highly technological carbon-based materials, such as carbon nanotubes [21], graphene, and graphite powder [22–24], as well as carbon black [25], have been considered to achieve this goal. However, the first additions used in this field with proven effectiveness were carbon fibers (CFs) [26]. CF technology has significantly evolved since the 1960s [27] and is currently the most used technology for the production of high-strength composites with a wide range of properties. Carbon filaments have a tensile strength of 4–6 GPa and a Young's modulus of up to 600 GPa [28]. Their fast diffusion in many industrial sectors has gradually decreased their production costs and has led to an increase in the volume of the by-products obtained by cutting and milling CF fabrics and panels. These wastes cannot always be reused within the same CF industry, but they can be used for the production of composite cementitious materials [29,30], thanks to their large production volume and low price.

Dispersed within the cement-based composites, CFs form a micro-filament network that supports the cement matrix subjected to stress conditions [31]. Their high aspect ratio leads to a high bridging effect, which increases the cracking toughness of the material [32]. A detailed work by Han et al. [11] studied the interaction between the CF and the cement matrix through microscopic and microstructural analyses, demonstrating that fibers can increase the flexural and compressive strength of mortars by 15% and 18%, respectively, up to a certain threshold. This study especially highlighted the effectiveness of 6 mm-long micro-fibers. Nguyen et al. [29] obtained similar results by studying mortars reinforced with different types of recycled CFs, observing an increase in their flexural strengths and fracture energies. Furthermore, Chung et al. [12,33] showed that the addition of CFs decreases the shrinkage deformations of the cement paste by 22%.

Chung et al. [26] were also the first authors to use CFs for the production of multifunctional cement-based materials (strain-sensitive composites) in the 1990s, thanks to their benefits in increasing the electrical conductivity. Since then, many authors have studied the effect of fibers within cement-based materials, which has led to the multi-phase behavior of the composites [34].

Both electrolytic and electronic conductive mechanisms are present within multi-phase materials, such as mortars or concretes with conductive fibers [35,36]. Electrolytic conductivity is related to the mobile ionic species that emerge from mixing the binder with the water [37], whereas the electronic conductivity is related to the transportation of free electrons through the conductive phase (carbon or metal fibers). The resistivity of the whole composite is, therefore, determined by the combination of both the electrolytic resistivity and the electronic resistivity [35].

Xie et al. [38] investigated the relationship between the fiber concentration and electrical conductivity of the composite, finding a significant reduction in the electrical resistivity by exceeding a certain addition threshold (the percolation theory) due to the increase in electrical contact paths between the fibers. An increasing amount of CFs also decreases the influence of the w/c ratio and the curing time on the electrical properties of the concrete, as shown by Chacko et al. [39].

Chiarello and Zinno [36] studied the influence of the dimensional characteristics of the conductive filaments, demonstrating that a higher length (greater aspect ratio) creates more effective electric paths with the same volume of addition. In particular, they showed that a 6 mm-long CF increases electrical conductivity up to two orders of magnitude than that of plain mortars. Six-millimeter-long fibers were also studied by other authors [40], such as Donnini et al. [41], who showed that an addition of CFs equal to 3% by volume decreases the electrical resistivity of the structural mortars from more than 45000 Ω·cm (reference mixture) to 110 Ω·cm.

Some of the most relevant studies supplied good results by using high concentrations of expensive conductive materials [42], which though make the composites difficult to produce at industrial scale. Furthermore, although a high dosage of conductive fibers increases the electrical properties of the cement-based material, it also leads to a gradual loss of workability and homogeneity of the mixture [41], with a consequent decrease of both mechanical and durability properties.

As referred, literature already reports many papers on fibers to improve the mechanical and/or electrical properties of mortars/concretes. However, generally, a single type of fiber is investigated and/or in a narrow range of concentrations.

The novelty of this study is to provide a comprehensive study on the compositional optimization of high-conductive multifunctional fiber-reinforced cement mortars (FRCMs). To this aim, the effects of three different fiber types, which have already shown good performance in the relevant literature, added at a broad range of concentrations, on the mechanical, electrical and durability properties of FRCMs have been compared. In particular, the effects of 6 mm-long virgin carbon fibers (VCFs) have been compared with those of less expensive and more sustainable recycled carbon fibers (RCFs), obtained by the cutting and processing of CF panels. Brass-plated steel fibers (BSFs), widely used for the reinforcement of cement-based materials, have been included, since they have also demonstrated to supply good electrical properties to mortars/concretes, according to many authors [43,44]. The wide range of fiber concentrations, considered in this work, includes both high dosages, from 0.8 to 1.6 vol.%, and low dosages, from 0.05 to 0.4 vol%, according to other scientific literature [41]. Therefore, this work aims to find the right compromise among mechanical, durability and electrical properties as a function of the fiber compositions of the examined FRCMs, developing a background for the research of the best mix, both in terms of performances and costs, for a given application.

The mechanical contribution of fibers has been evaluated by compressive and tensile splitting strength tests, and by studying the pre- and post-cracking flexural behavior of the composites. The durability of the mortars has been assessed by means of capillary water absorption and free drying shrinkage tests. The study of the electrical conductivity of fiber-reinforced mortars requires a careful setup of the tests, due to their multi-phase composition [35]. Therefore, in order to identify the different electrical contribution of the fibers and the cement matrix on the electrical properties of the manufactured composites, an accurate assessment of their electrical resistivity has been performed by means of electrochemical impedance spectroscopy (EIS).

2. Materials and methods

2.1 Materials

A commercial CEM I 52.5R Portland cement was used as a binder. As an aggregate, silica sand with grain size ≤1 mm was used. The use of a fine binder and fine aggregate is recommended by several studies [15,45], in order to obtain better workability for the fresh mixture (especially with high fiber contents) and high compactness for the hardened composite. The aggregate/cement (a/c) ratio and the water/cement (w/c) ratio of the mortars were equal to 1.5 and 0.5, respectively, according to the relevant literature [41,46].

Three different types of conductive micro-fibers with an average length of 6 mm were used: short cut virgin carbon fibers (VCFs) SFC-EPB from STW GmbH, recycled carbon fibers (RCFs) CGF-6 from APPLY CARBON SA, and brass-plated steel fibers (BSFs) Dramix® OL6/.16 from BEKAERT.

Microscopic and elementary chemical analyses of fibers were performed through a PHILIPS XL20 Scanning Electron Microscope (SEM) and Energy Dispersive X-ray analyses (EDX), respectively. The results are shown in Fig. 1 and Table 1. The SEM images highlight the high morphological uniformity of VCFs, while the RCF surface is covered by carbon micro-fragments, generated by the industrial processes of cutting and milling. BSFs show indented ends caused by the cutting operations.

The properties of the three different types of fibers are shown in Table 2.

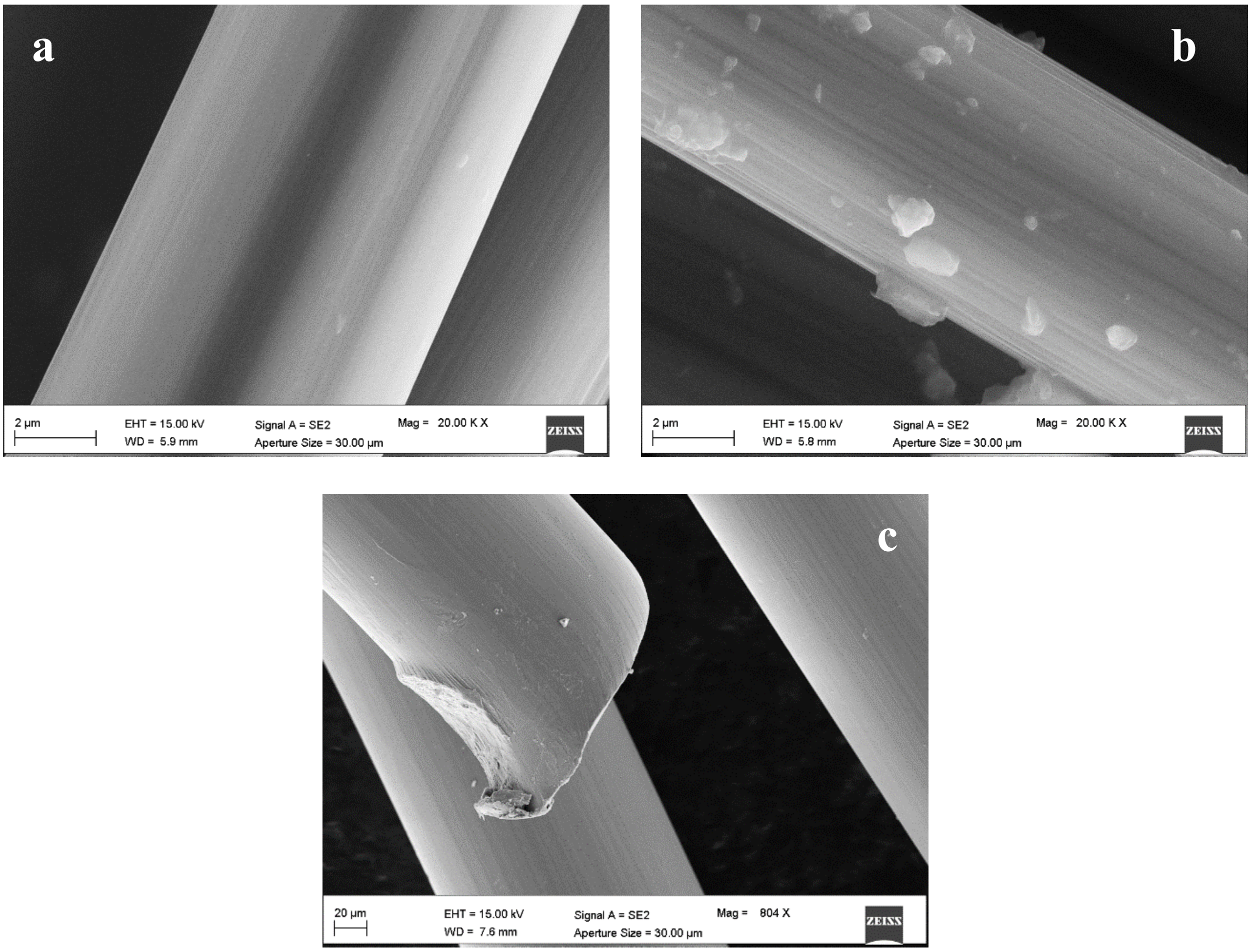

Fig. 1. SEM images of the conductive fibers: A) VCF, B) RCF, C) BSF.

Table 1. Elementary analysis of conductive fibers (wt.%) by EDX.

	VCF	RCF	BSF
C	> 92.0	94.0	3.1
Fe	-	-	52.4
Cu	-	-	27.8
Zn	-	-	15.4
O	-	-	1.3

Table 2. Properties of conductive fibers (from data sheets).

	VCF	RCF	BSF
Commercial name	SFC-EPB	CFG-6	OL 6/.16
Surface coating	Epoxy	Glycerol	Brass
Average diameter (μm)	7.0	7.0	160.0
Average length (mm)	6.0	6.0	6.0
Aspect ratio	857	857	38
Density (g/cm^3)	1.78	1.70-2.00	7.87
Specific surface area (m^2/g)	0.229	0.195	0.003
Young's modulus (GPa)	230-250	230	200-210
Tensile strength (MPa)	4000	3500	2600
Price (€/kg)	59.50	20.00	4.00

The fibers were added in 7 different concentrations, expressed as the volume percentage of the manufactured mortars: 4 with low amounts, equal to 0.05, 0.1, 0.2, 0.4 vol%, and 3 with high amounts, equal to 0.8, 1.2, 1.6 vol%, which showed high performance in other works [41]. Since the supplier reports a variable density range of recycled CF (1.7-2.0 g/cm^3) an average value of 1.85 g/cm^3 has been used for the calculation of the volume percentages. The wide range of fiber dosages has the aim to find the right compromise among workability, mechanical, durability and electrical properties of the FRCMs.

To facilitate the mixing of the mortars with high CF content, a high-performance polycarboxylate ether-based superplasticizer (SP) Melflux® 4930F (BASF SE) was added, until reaching a mixture classifiable as "plastic mortar", according to UNI EN 1015-3:2007. Overall, 22 different mortar mixes were produced (Table 3), including a plain mixture without fibers, manufactured as reference (REF). The mix proportions of the mortars are listed in Table 3.

Table 3. Mix proportions of mortars.

Mixtures	OPC (g/L)	Water (g/L)	Sand ≤ 1mm (g/L)	Fibers (g/L)			SP (g/L)	w/b	Fibers volume (cm^3/L)
				VCF	RCF	BSF			
REF	720	360	1080	-	-	-	-	0.5	-
0.05VCF	720	360	1080	0.9	-	-	-	0.5	0.5
0.1VCF	720	360	1080	1.8	-	-	-	0.5	1.0
0.2VCF	720	360	1080	3.6	-	-	-	0.5	2.0
0.4VCF	720	360	1080	7.3	-	-	-	0.5	4.0
0.8VCF	720	360	1080	14.5	-	-	6.6	0.5	8.0
1.2VCF	720	360	1080	22.0	-	-	9.4	0.5	12.0
1.6VCF	720	360	1080	29.0	-	-	12.9	0.5	16.0
0.05RCF	720	360	1080	-	0.9	-	-	0.5	0.5
0.1RCF	720	360	1080	-	1.8	-	-	0.5	1.0
0.2RCF	720	360	1080	-	3.6	-	-	0.5	2.0
0.4RCF	720	360	1080	-	7.3	-	-	0.5	4.0
0.8RCF	720	360	1080	-	14.5	-	6.6	0.5	8.0
1.2RCF	720	360	1080	-	22.6	-	9.4	0.5	12.0
1.6RCF	720	360	1080	-	30.3	-	12.9	0.5	16.0
0.05BSF	720	360	1080	-	-	4.0	-	0.5	0.5
0.1BSF	720	360	1080	-	-	8.0	-	0.5	1.0

0.2BSF	720	360	1080	-	-	16.1	-	0.5	2.0
0.4BSF	720	360	1080	-	-	32.2	-	0.5	4.0
0.8BSF	720	360	1080	-	-	64.3	-	0.5	8.0
1.2BSF	720	360	1080	-	-	96.3	-	0.5	12.0
1.6BSF	720	360	1080	-	-	128.3	-	0.5	16.0

The OPC, sand and SP powder, if required, were initially stirred by manual mixing, and, subsequently, water was added. During blending, through a Hobart mixer, fibers were gradually added within the mortar, and the final composite was mixed at a variable speed for at least 5 min. This mixing procedure is aimed to obtain an optimal dispersion of the fibers, according to the literature [41,47], as shown in Fig. 2. The fresh mortars were poured into metallic molds, 40 x 40 x 160 mm in size, also using the mechanical vibration, to facilitate the compaction and the decrease of the amount of air bubbles.
The mortar specimens were cured for 2 days in the molds and maintained under controlled environmental conditions at T = 20 ± 1 °C and RH = 95 ± 5%. Subsequently, they were maintained at the same conditions out of the molds by wrapping them in a plastic film for 5 days. After 7 days, the plastic film was removed and specimens were maintained at T = 20 ± 1 °C and RH = 50 ± 5% until testing.

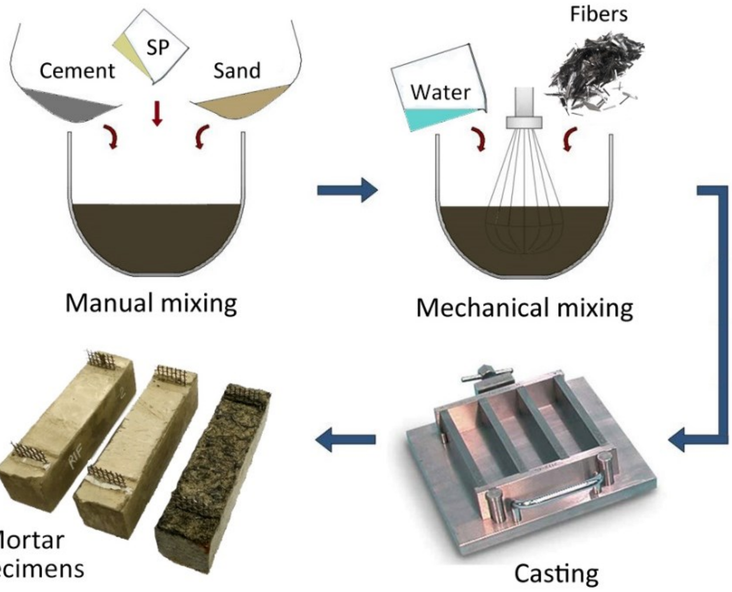

Fig. 2. Mixing procedure of mortars.

2.2 Methods

2.2.1 Characterization of the fresh mortar

The workability degree of the fresh mixtures was evaluated by means of a flow table test and the calculation of the relative percentage consistency, according to the UNI EN 1015-3 standard.

2.2.2 Mechanical tests

The effect of fibers on the mechanical properties of the mortars was investigated by flexural (R_f), tensile splitting (f_{ct}) and compressive (R_c) strength tests on 40 x 40 x 160 mm mortar specimens at 28 days of curing, according to UNI EN 1015-11 and UNI EN 123906 standards.

2.2.2.1 Crack Mouth Opening Displacement

The contribution of fibers on the post-cracking behavior of mortars was investigated by means of three-point bending tests with Crack Mouth Opening Displacement control (a CMOD test), according to the UNI EN 14651 and RILEM TC-50 standards. A notch was performed on 40 x 40 x160 mm mortar specimens with 10 mm of depth (1/4 of the section height) and 1 mm of thickness, and its opening under load was measured by means of an extensometer [48]. From the σ_f (MPa) vs. CMOD (mm/m) curves, the values of the elastic modulus E_f (slope of the initial section of the curve) and cracking toughness (subtended area of the curve) were calculated.

2.2.3 Durability tests

2.2.3.1 Water absorption

The tendency of the mortars to be infiltrated by aggressive agents was assessed via capillary water absorption tests on 40 x 40 x 80 mm specimens. The residual moisture content was removed after 28 days of curing by slow drying in an oven at 60 °C, until a constant mass was reached. The effect of fibers on the resistance to capillary absorption was evaluated by measuring the absorption coefficient (C) of the hardened composites for a short period (90 min) along with the water absorbed per unit area (Q_i) during a long period (8 days), according to the UNI EN 1015-18 and UNI EN 15801 standards, respectively. The results obtained by these tests are very important considering that water is the main carrier for the ions transport, including the aggressive ones (e.g., Cl^- and SO_4^{2}) [49].

2.2.3.2 Shrinkage

Hygrometric shrinkage greatly affects the durability of concrete, since it promotes mechanical stress due to the different drying speeds between the surface and the internal areas, thereby leading to cracking in the presence of mechanical constraints, such as reinforcing bars [50,51]. In this work, the effect of fibers on the free drying shrinkage of mortars was assessed by measuring the axial strain of 40 x 40 x 160 mm mortar specimens starting from the day after casting and during 3 months of curing (according to UNI EN 12617-4). Specimens were exposed to T = 20 ± 1 °C and RH = 90 ± 5% for the first 24 h and then to T = 20 ± 1 °C and RH = 50 ± 5%; the percentage of weight loss due to water evaporation was calculated during the test period [52].

2.2.4 Porosity and microstructural characterization

The porosimetric properties of the mortars after 28 days of curing were investigated through a mercury intrusion porosimeter (MIP) Thermo Fisher 240 Pascal, by analyzing the pore distribution and calculating the total porosity (V_p) and the average pore diameter (d_p). The mortars' microstructures and the interface between the cement matrix and fibers were observed by using an SEM PHILIPS XL20. Both analyses were performed on dried mortar specimens, treated as described in section 2.2.3.1.

2.2.5 Electrical conductivity

The electrical properties of the mortars were studied through electrochemical impedance spectroscopy (EIS) by means of a Gamry Reference 600 potentiostat [41]. The electrical resistivity (ρ) was determined after 2, 7, 14, 21, 28, 49, 70, and 91 days of curing. In the manufactured mortar specimens (Fig. 2), just after the casting, two stainless steel meshes #6 (3.5 mm of aperture and 0.71 mm of wire diameter) were vertically inserted to use them as electrodes for the tests. As in many works [41,53], stainless steel meshes were preferred to flat sheets, within the cement paste, for minimizing specimen discontinuities in correspondence of their position.

These two electrodes had a total extension area of 30 x 50 mm^2, with 30 x 30 mm^2 area inside the specimen. They were placed at a distance of 120 mm (Fig. 3) in order to measure the impedance of the different mortars as a function of the curing time. The distance–area ratio defines the so-called cell-constant K, expressed in cm^{-1}, of the electrochemical cell constituted by the two electrodes immersed in the mortar. This parameter cannot be obtained by a simple geometrical calculation of distance/area, considering, in particular, that both electrodes are meshes and not flat sheets. K can be determined by using an electrochemical cell that has the same geometry of the specimen with both electrodes, as shown in Fig. 3, on the left, where in place of the cement-based material, a solution of known conductivity (or resistivity) is present in the cell. The solution used for the determination of K was a 0.01M KCl solution, which gave a calculated cell-constant (K) equal to 0.7681 cm^{-1}.

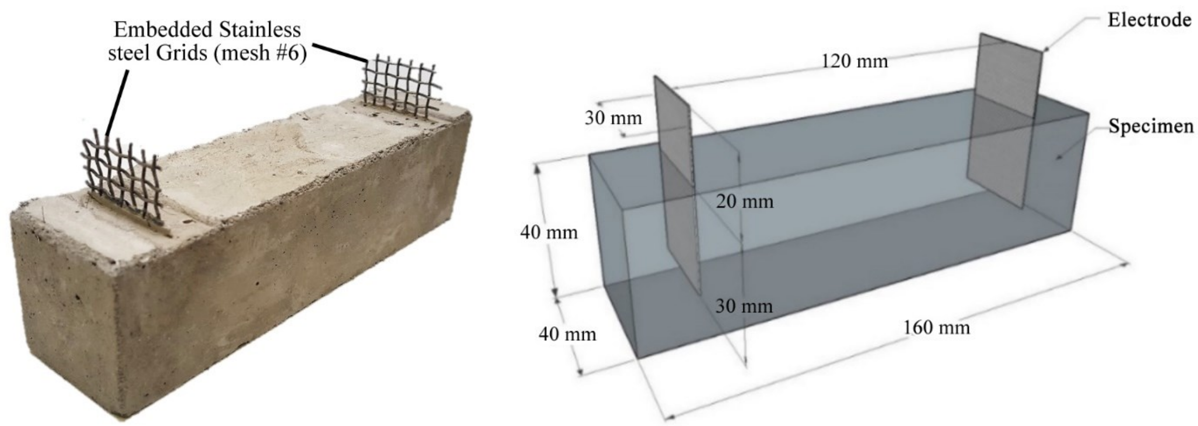

Fig. 3. The view (left) and dimensions (right) of specimens produced for electrical conductivity tests.

EIS techniques, particularly with high-frequency electrical signals, are widely used in the literature to measure the electrical resistivity of cement-based composites [41,54], because it allows to exclude or, at least, to minimize polarization effects of the embedded electrodes.

Impedance measurements on the mortar specimens were performed by connecting one mesh-electrode to the working cable and the working sense cable (W-WS) of the potentiostat and the other mesh-electrode to the counter cable (C), short-circuited with the reference (R) cable [35].

The EIS measurement scan was performed with an AC signal amplitude of 10 mV rms, in a frequency range starting from 1 MHz up to a lower limit of 10 Hz by setting 10 points/decade. The raw EIS data were processed through an Excel macro, which selects the values of the impedance moduli, in terms of log |Z|, to which correspond phase values close to zero (the "resistive behavior" of the mortar), and calculates the average log |Z| among the selected data. The data with these characteristics were found particularly in the middle and high frequency ranges of the obtained EIS spectra. Considering that in the real measurements, a phase equal to zero cannot be reached, a phase angle threshold (PAT), as close as possible to zero was set for selecting the impedance data, as the Bode plot of Fig. 4 shows.

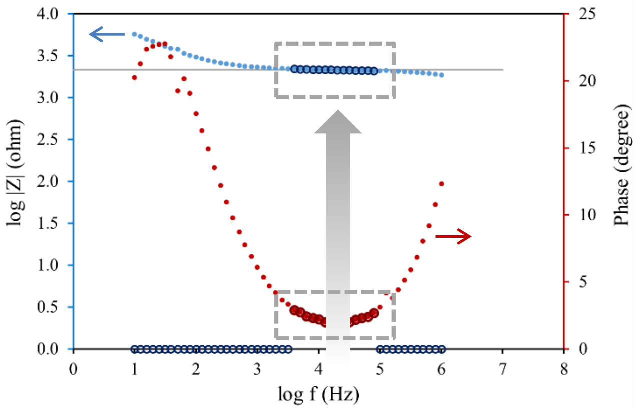

Fig. 4. Example of a Bode plot, corresponding to the REF mortar, to show the data processing: the average value of log |Z| is calculated from the values (circled blue points) selected by fixing a PAT value close to 0° (circled red points).

From the log |Z| average value, the electrical resistance R (Ω) of the composite specimen was calculated using Eq. (1):

$$R = 10^{\overline{\log|Z|}}. \quad (1)$$

Successively, the electrical resistivity ρ (Ω·cm) of the mortars was calculated, according to the second Ohm's law (Eq. 2):

$$\rho = R\frac{A}{l} = \frac{R}{K} \quad (2)$$

where K is the above-mentioned cell constant.

3. Results and discussion

3.1 Mechanical and microstructure properties

The addition of fibers within the mortars led to a noticeable increase in mechanical resistances, particularly in flexural and tensile strength. The comparison between the ultimate mechanical performance of the mortars after 28 days of curing is shown in Fig. 5.

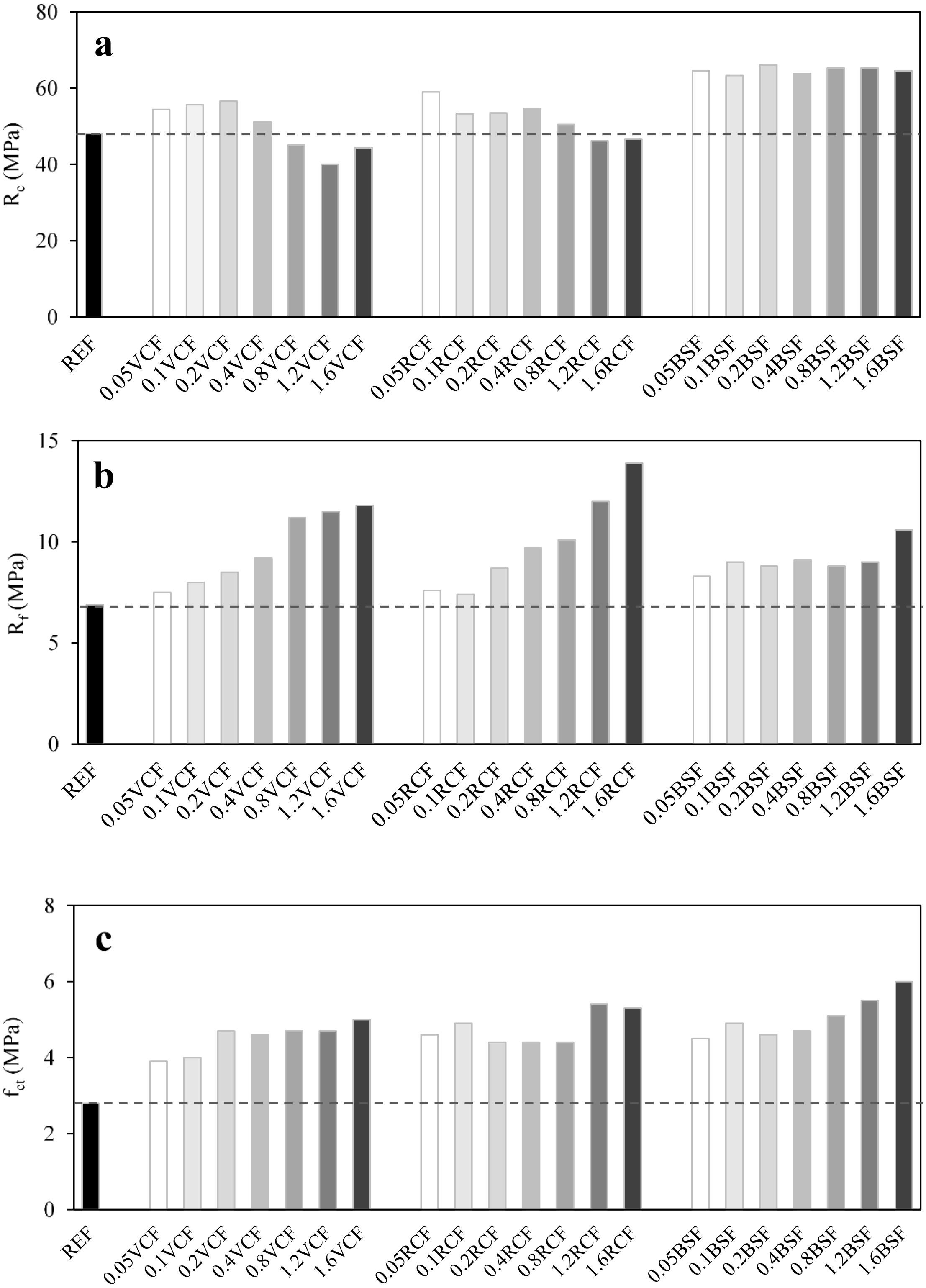

Fig. 5. Comparison between compressive (a), flexural (b) and splitting tensile (c) strength of mortars at 28 days of curing.

The results show that a low amount of CFs (up to 0.4 vol.% for VCFs and 0.8 vol.% for RCFs) leads to an enhancement in compressive strength (Fig. 5a), whereas slight decreases are detected in mortars containing high concentrations of VCFs and RCFs (up to -17% for 1.2 VCFs). Contrariwise, all mortars reinforced with BSFs show higher R_c values than the REF one, with an increase of 38%, regardless of the fiber content. These results are related to the specimen's structures. In fiber-reinforced mortars and concretes, the mechanical compression behavior is influenced by the technical properties of the filaments (e.g., the aspect ratio) but also by other factors, such as the density of the reinforcing material [55]. In the case of CFs, the addition of filaments into the cement mortar up to a certain percentage enhances the mechanical properties thanks to the ability of CFs to prevent the growth of micro-cracks. However, when the carbon fiber content is too high, they tend to clump and cause air voids, thereby reducing mechanical compressive strength [11,41]. This phenomenon does not occur with BSFs, since at the same volume content of CFs, BSFs are less numerous due to their lower aspect ratio (Table 2, Fig. 6), which allows a better dispersion within the matrix, even in large amounts.

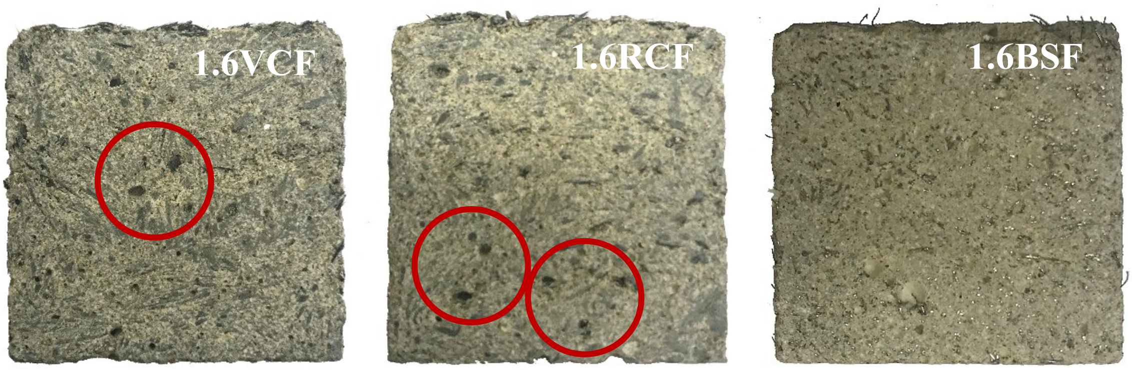

Fig. 6. Section of 1.6VCF and 1.6RCF specimens, where the agglomerated CFs clumps are clearly visible, which cause air voids within the composite (red circle). Section of 1.6BSF shows a more uniform structure.

Concerning R_f, all types of fibers provide a prominent increase in strength related to the number of filaments (the higher the fiber concentration, the higher the R_f values), although this effect appears less evident for BSFs (Fig. 5b). The highest R_f values were obtained by RCFs, with increases up to 200% (mixture 1.6 RCF) compared to REF mortar. The best mechanical properties of CFs compared to those of BSFs are related to their higher aspect ratios (Table 2). As widely demonstrated in the literature, the aspect ratio of fibers has a considerable influence on the mechanical properties of fiber-reinforced composites [56,57]. CFs, at the same volume percentage as the added BSFs, create more connections, amplifying the stitching effect in the presence of micro-cracks, the adhesion forces, and the bridging effect [58].

Similar results were obtained from tensile splitting strength tests (Fig. 5c). Generally, f_{ct} values increase by increasing the fiber content, although this trend is less evident than in the flexural strength test. All FRCMs (even those with low fiber concentrations) show higher mechanical resistance than the reference, with increases ranging from 36% to 111% (for 1.6 BSF mortar).

The RCFs led to significant increases in mechanical performance, with greater flexural strengths than both VCFs and BSFs. The mortars' microstructures and the interaction between fibers and the cement matrix were analyzed through SEM observations. In Fig. 7, mortars with the same content of fibers, equal to 0.8 vol%, are reported.

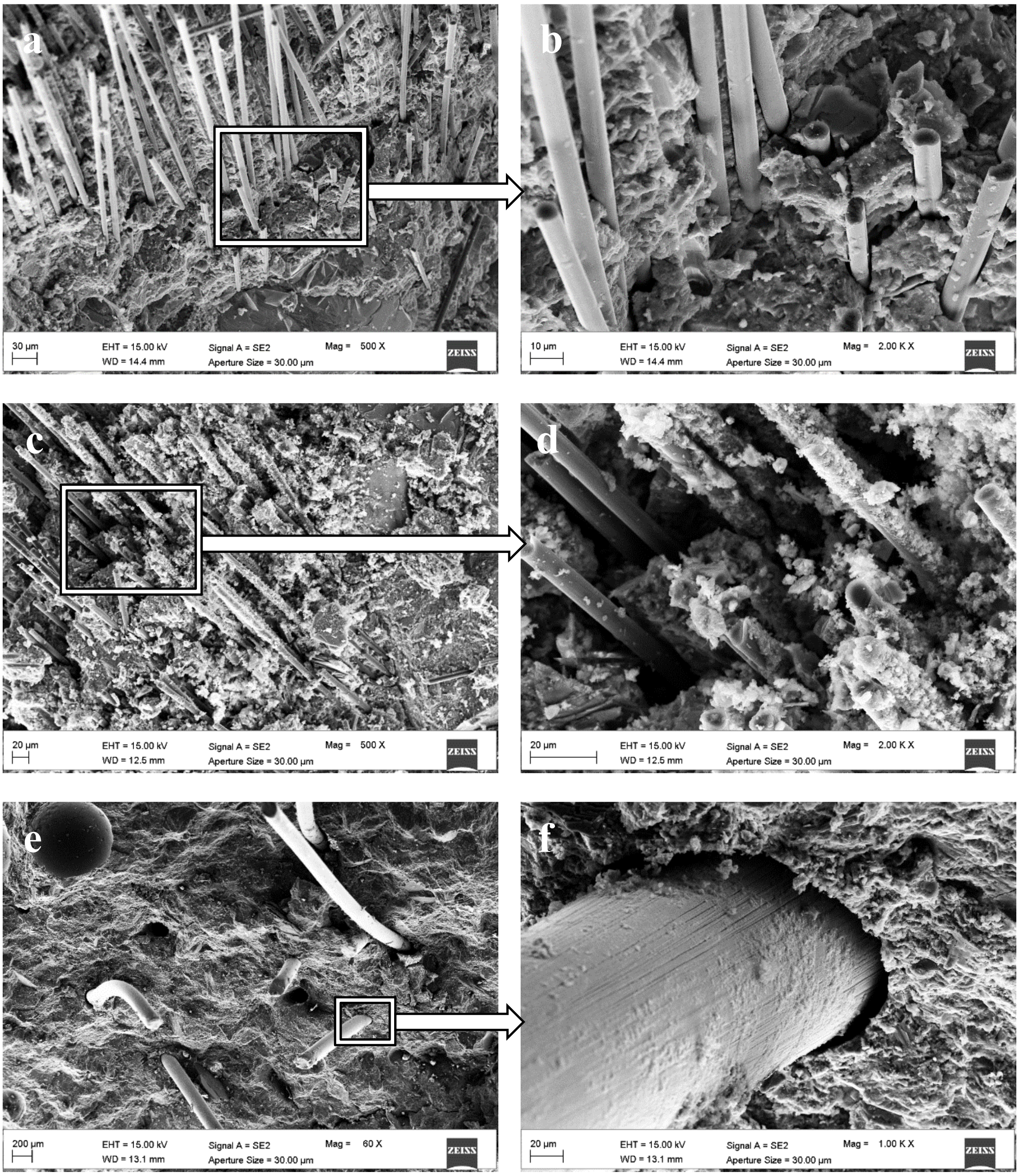

Fig. 7. SEM observations: Fiber agglomerates (left) and enlargement on fibers-cement matrix interface (right): a-b) VCF, c-d) RCF, e-f) BSF.

The images show that, at this volume content of fibers, CFs are effectively incorporated within the cement paste (Figs. 7a-d). More specifically, RCFs are covered by cement paste particles (Figs. 7c–d), as detected by EDX analysis. As seen in Fig. 1, RCFs show a high presence of carbon micro-particles, which increase the specific surface of the RCFs, thus working as nucleation points for the formation of C-S-H crystals on the filaments [59]. This explains the better interaction between the RCFs and the cement matrix [29,59], as well as their high mechanical performance under flexure. Mortars containing BSFs show a worse interface between the fibers and the cement paste (Fig. e-f), which is responsible for the lower flexural strength values than those of the RCF-based mortars. On the other hand, the lower number of filaments (at the same volume percentage), owing to the lower aspect ratio of the BSFs (Table 2), leads to a greater homogeneity of the cement paste and higher compressive strength (Fig. 5a).

3.1.1 Post-cracking behavior

The CMOD test provided additional information regarding the effect of fibers on the post-cracking behavior of mortars. Mixtures with high fiber concentrations (i.e. 0.8, 1.2, and 1.6 vol.%) showed the most significant results. Fig. 8 shows the corresponding relationship between flexural stress σ_f and opening displacement, from which the values reported in Table 4 have been calculated. The results relative to REF and low-fiber mortars are not shown in the graph because they did not show any significant post-cracking behavior.

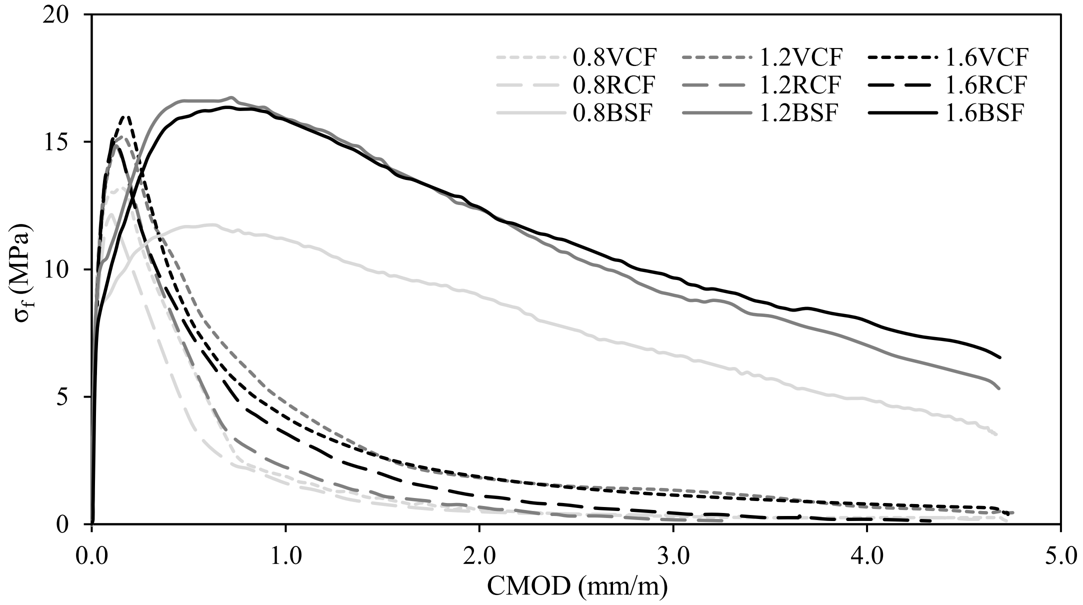

Fig. 8. Flexural stress vs. CMOD of mortars with high fiber concentrations (i.e. 0.8, 1.2 and 1.6 vol. %).

Table 4. Post-cracking parameters of mortars.

Mixtures	Ultimate CMOD (mm)	E_f (MPa)	Toughness (MPa)
REF	0.020	22.9	-
0.8VCF	0.155	20.6	8.8
1.2VCF	0.170	17.7	15.2
1.6VCF	0.190	15.7	14.7
0.8RCF	0.106	16.8	7.2
1.2RCF	0.132	17.8	9.0
1.6RCF	0.113	18.1	11.2
0.8BSF	0.641	20.7	37.1
1.2BSF	0.724	24.2	52.5
1.6BSF	0.719	20.9	53.6

The curves show different behaviors for the mortars related to the different nature of the fibers. The mortars reinforced with CFs show a high flexural Young's modulus [47] but also a high brittleness, as demonstrated by their sharp peaks and low ultimate CMOD values. On the other hand, BSFs greatly increase the flexural toughness of the mortars (up to 54 MPa), with high crack opening values before breaking. This effect is probably linked to the high intrinsic flexural stiffness of SFs, due to their larger diameter. Indeed it is demonstrated that a larger SF diameter increases the cracking toughness and the maximum crack opening [60]. Furthermore, the ends of the BSFs are hooked (Fig. 1c), thereby increasing their pull-out resistance during the tensile stress.

3.2 Porosity and capillary water absorption

Porosimetric analyses were performed on mortars containing both one low and one high fiber amount, namely 0.1 and 0.8 vol.%, and on the REF mortar. The calculated total porosity volume (V_p) and average pore diameter (d_p) are reported in Table 5, whereas the cumulative pore diameter is shown in Fig. 9.

Table 5. Total porosity volume (V_p) and average pore diameter (d_p) of mortars.

Mixtures	V_p (%)	d_p (μm)
REF	21.3	0.080
0.1VCF	18.7	0.074
0.8VCF	15.1	0.052
0.1RCF	19.3	0.068
0.8RCF	15.0	0.056
0.1BSF	17.5	0.071
0.8BSF	15.3	0.068

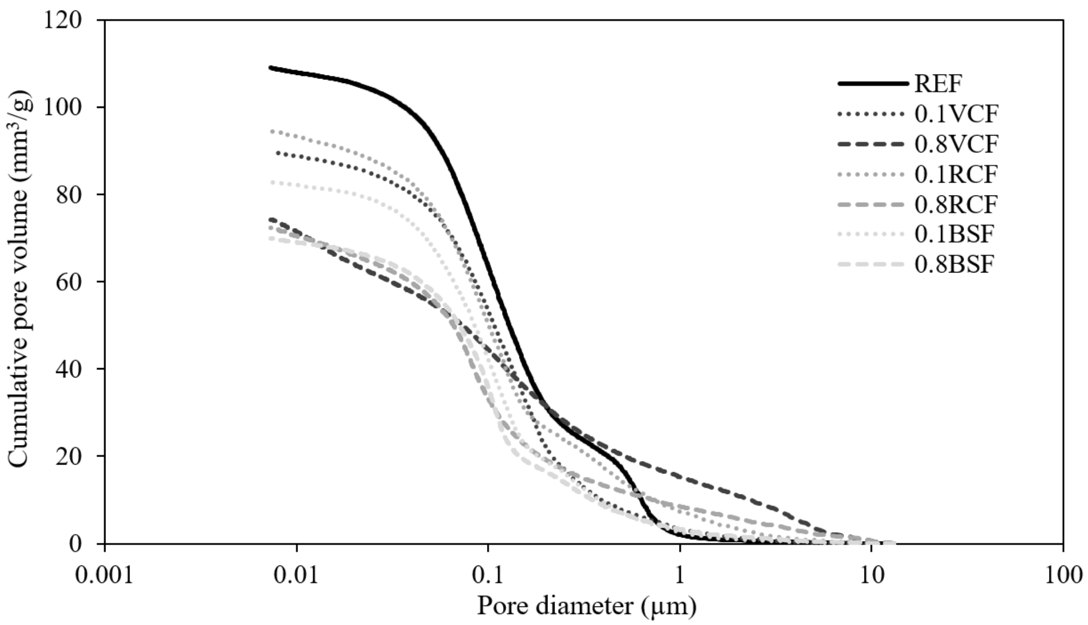

Fig. 9. Pore size distribution of mortars.

The results show that all types of fibers reduce the total volume of the capillary pores. The addition of 0.8 vol% CFs and SFs decreases the total volume of the micro-pores by approximately 29% (Table 5). Both the pore volume and the critical pore diameter are related to the amount of fibers, since the greater the concentration of fibers, the lower the V_p and d_p values. The relation between the increase in the amount of CFs and the decrease in the porosity of cement-based materials has been proven by other authors [61]. The fibers improve the microstructure of the composite mortar, since the filaments show a good adhesion with the cement paste (Fig. 7) and act as nucleation points for the formation of hydration products, thus reducing the micropores [11]. It is worthy to notice that a higher presence of fibers also reduces the formation of micro-cracks [40] (which are interpreted by MIP as equiaxed pores).

However, at a high-volume content of CF, the volume of the pores with large diameters (between 1 and 10 µm) increases, owing to the difficult compaction of mortars, which also leads to the reduced compressive strength of the mortars (Fig. 5a).

From the water absorption tests, the absorption coefficient (C) and the amount of water absorbed per unit area as a function of time (Q_i) were calculated and the results displayed in Figs. 10 and 11, respectively.

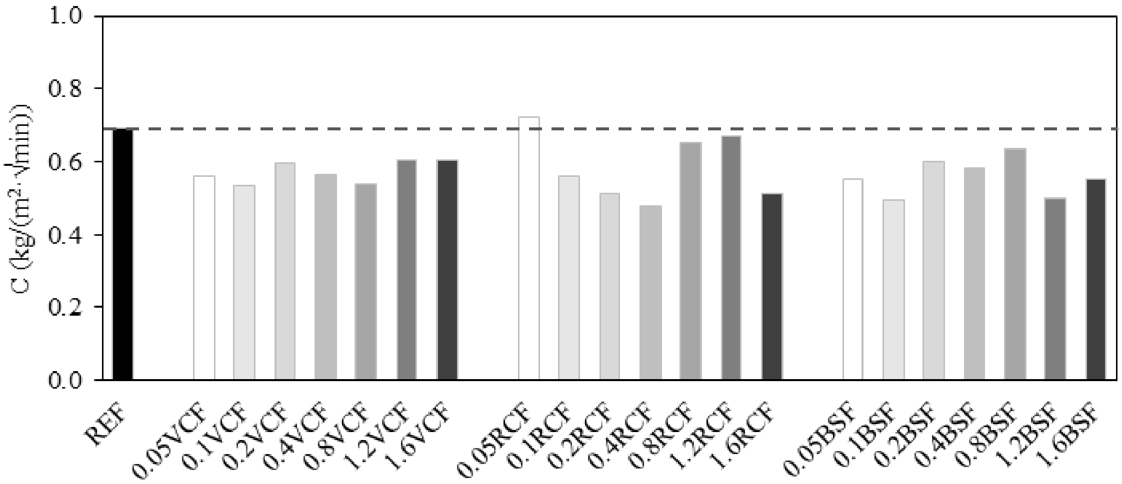

Fig. 10. Water absorption coefficient (C) of mortars at 28 days of curing.

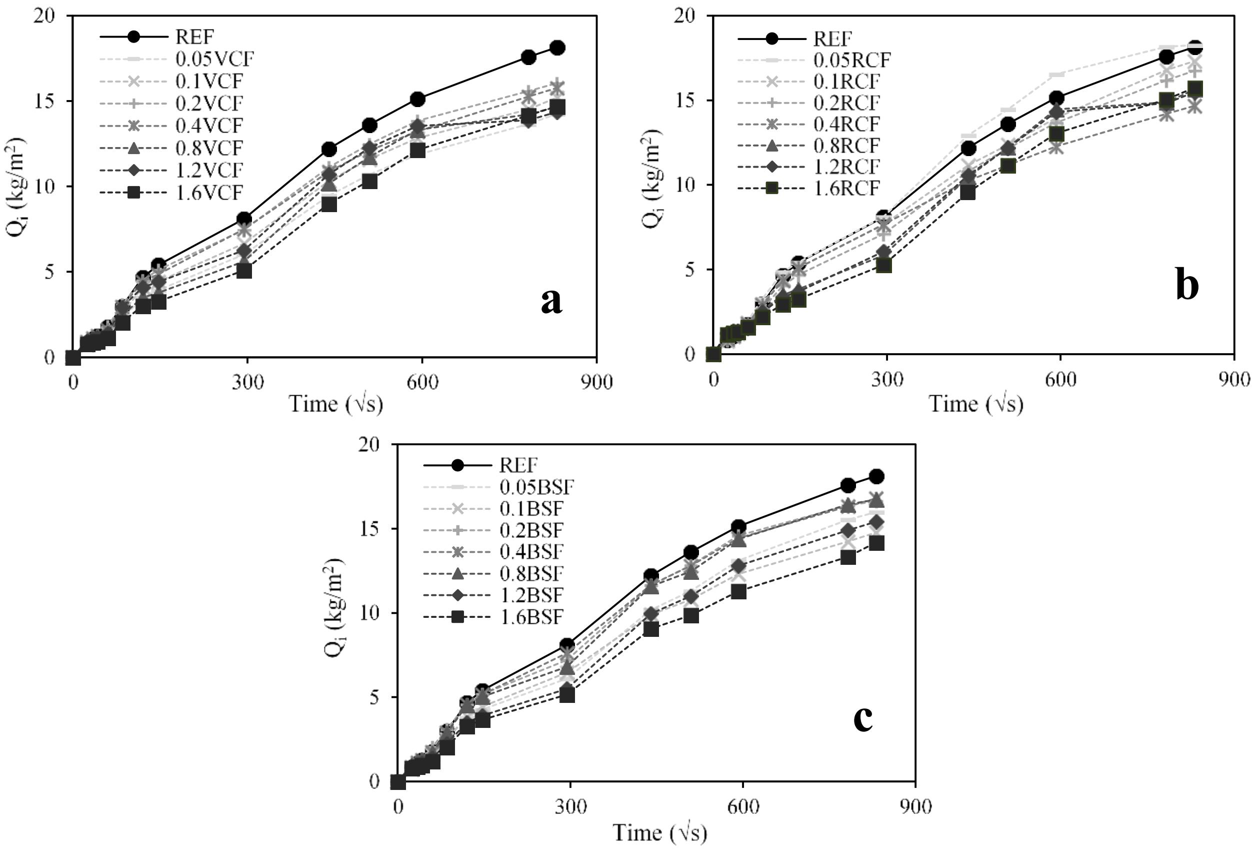

Fig. 11. Water absorbed per unit area (Q_i) of mortars reinforced with: A) VCF, B) RCF, C) BSF compared to REF.

From the results, the addition of fibers clearly leads to a reduction in water absorption, both during short and long periods of time. Almost all FRCMs show lower absorption coefficients (Fig. 10) than the REF, although the values are by no means related to the type and amount of fibers.
The effect of the fiber amount is more evident in the long-period tests, where a higher concentration of filaments leads to a lower volume of absorbed water (Fig. 11). The least permeable mixtures are 1.6 VCF (Fig. 11a) and 1.6 BSF (Fig. 11c), with Q_i values 22% lower than the REF. However, all FRCMs show lower Q_i values than the plain mortar.
The greater impermeability of the FRCMs is related to the lower volumetric amount of their capillary pores, particularly those with diameters <1 μm, which are voids that mainly promote water absorption [62].

3.3 Drying shrinkage

The drying shrinkage results are reported in Fig. 12.

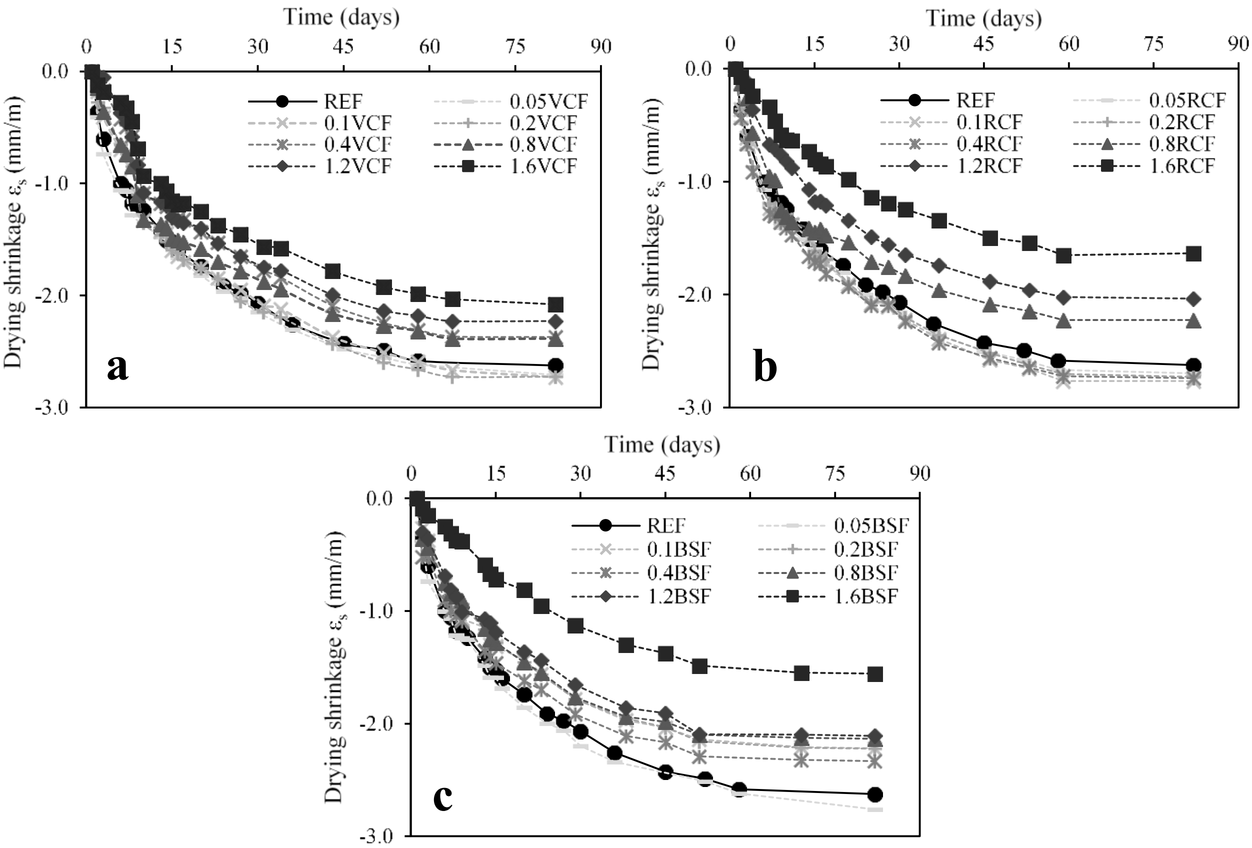

Fig. 12. Drying shrinkage (ε_s) of mortars reinforced with: A) VCFs, B) RCFs, C) BSFs compared to REF.

The curves show that the drying shrinkage of the mortars stabilizes after 60 days of curing. Mortars with low carbon fiber contents show deformation curves similar to those of the plain mixture, while high fiber concentrations lead to significant decreases in drying shrinkage during the whole curing period. It is evident that, for all types of fibers, the higher the concentration of fibers, the lower the shrinkage strain of the mortars [12,63]. The largest reductions were measured in mortars with a high content of RCFs and BSFs (1.6 RCF and 1.6 BSF), which have ultimate ε_s values 38% lower than the reference (Figs. 12b–12c).

The low drying shrinkage of the FRCMs is linked to their microstructures. It is well known that shrinkage is strongly influenced by the surface tension generated by water loss within capillary pores [64], which generates attraction forces between the hydrated cement particle surfaces (mainly C-S-H), which in turn determines the drying shrinkage [62]. A lower volume of FRCM capillary pores leads to a substantial reduction in their shrinkage strain. In particular, mortars with high amounts of CFs and SFs are characterized by a very low volume of pores with diameters <0.1 μm (Fig. 9), the configuration most responsible for drying deformation [50,65].

Usually, shrinkage is closely related to the weight loss of the material over time, since the greater the amount of water lost during the curing period, the higher the tension stress within the pores. The amount of water lost by the specimens during the curing period is given in Fig. 13.

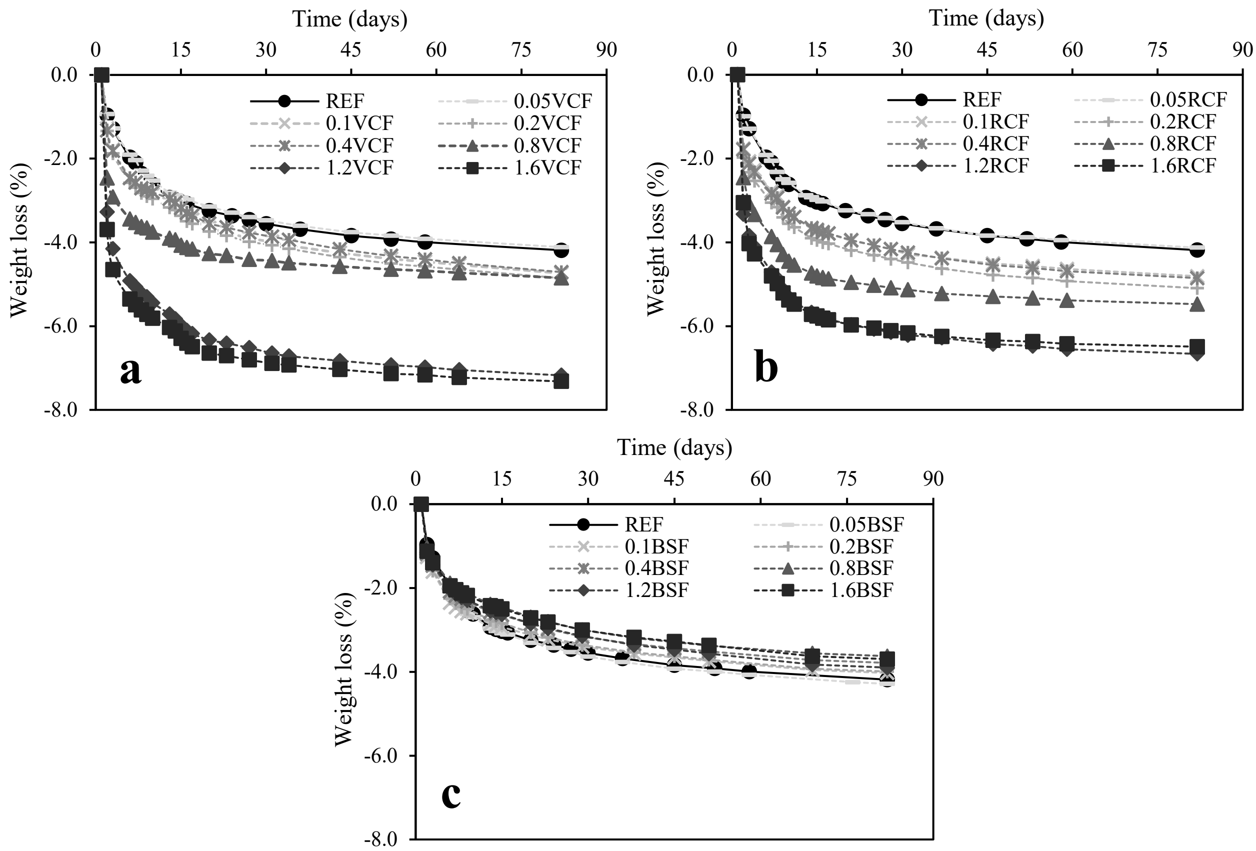

Fig. 13. Weight loss (%) during the curing period of mortars reinforced with: A) VCF, B) RCF, C) BSF compared to REF.

As can be seen, the water lost by mortars with a high CF content is much higher than that of mortars with BSFs and the REF, particularly during the first days of curing. The 1.6 VCF and 1.6 RCF show, respectively, ultimate water losses that are 75% and 55% higher than those of the reference mortar. These mortars show an uncommon weight loss-ε_s relationship, since the greater the concentration of CFs, the greater the amount of water evaporation (Fig. 13) but the lower the shrinkage deformation (Fig. 12). This phenomenon confirms the high presence of pores with large diameters (between 1 and 10 μm) within the mortars with high CF concentrations (Section 3.1). The high presence of mixing water contained within the large-size pores leads to high weight losses for the specimens with CFs during the first curing period. However, large diameter voids do not significantly affect shrinkage deformations [64], which, in mixtures with a high content of VCF and RCF, are very low.

3.4 Electrical characterization

The electrical properties of cement-based composites require an analysis of the impedance spectra obtained from EIS measurements performed on FRCMs. As mentioned in the introduction section, both the electrolytic and electronic conductive mechanisms of multifunctional cement-based materials lead to significant differences between the values of impedance found along the whole frequency range after EIS measurements. In more detail, at low frequencies, the effect of the polarization of the stainless steel electrodes gives a response greater than that of the cement-based composites, while at high frequencies, the electrical contribution of the fibers combined with that of the matrix becomes more important than that of the electrodes [35]. This different response is visible through the use of the EIS technique, which is widely used to investigate the dielectric/conductive behaviors of cement-based materials [66–70]. In the Nyquist plot, the impedance Z is reported as -Z_{Im} vs. Z_{Re}, and, in particular, the electrical resistance of a plain cement-based material is determined around a cusp (Fig. 14) formed by two arcs, describing the electrical behavior of the cement-based material (high frequencies, “material arc”), where only the electrolytic characteristics of this material respond to the alternating current (AC) perturbations during the EIS measurements and the polarization effects on the electrode interfaces (low frequencies; the “electrode arc”) [71]. Corresponding to this cusp, the average value of R_m can be determined.

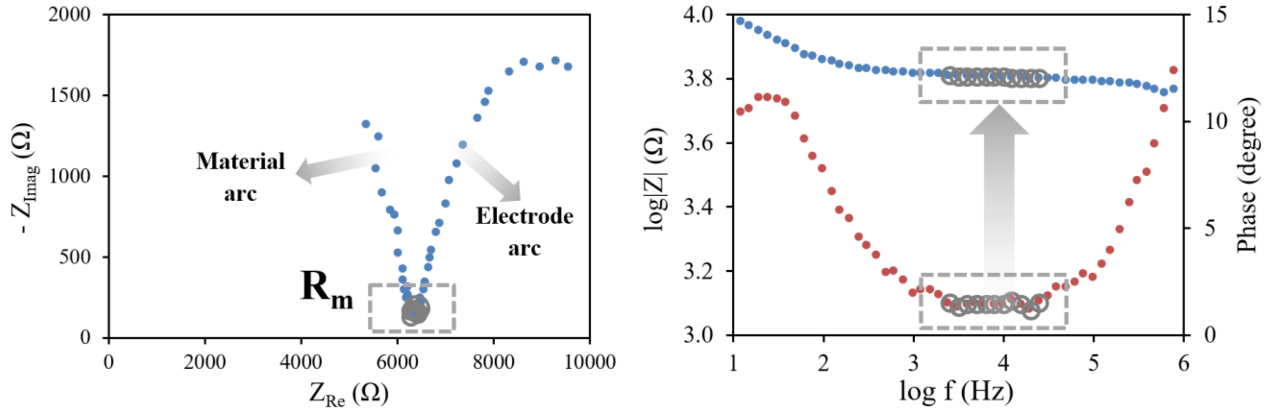

Fig. 14. Nyquist (left) and Bode (right) plots of a plain mortar (REF) showing the points used for R_m calculation (circled ones), in correspondence of the cusp, by means of the Excel macro mentioned in the section 2.2.5.

The addition of conductive fibers in the cement-based matrixes determines the appearance of a third arc in the Nyquist plot of the impedance spectrum of the new composite material, as shown in Fig. 15 compared to Fig. 14, as well as the appearance of two cusps: the first one, at high frequencies, is associated with the resistance of the composite material with the fibers (R_c), in which both the electrolytic (ions in the matrix) and electronic (electrons in the fibers) conduction mechanisms are present; the second one, at middle frequency range, is the resistance of the matrix (R_m), described above for the plain mortar [35,72–76].

This effect of the fibers on composite material is also clearly visible in the Bode plot (Fig. 15b), where the different impedance values are related to two different frequency ranges, after fixing a PAT close to 0°, corresponding to two distinct set of points, where the values of R_c and R_m can be obtained.

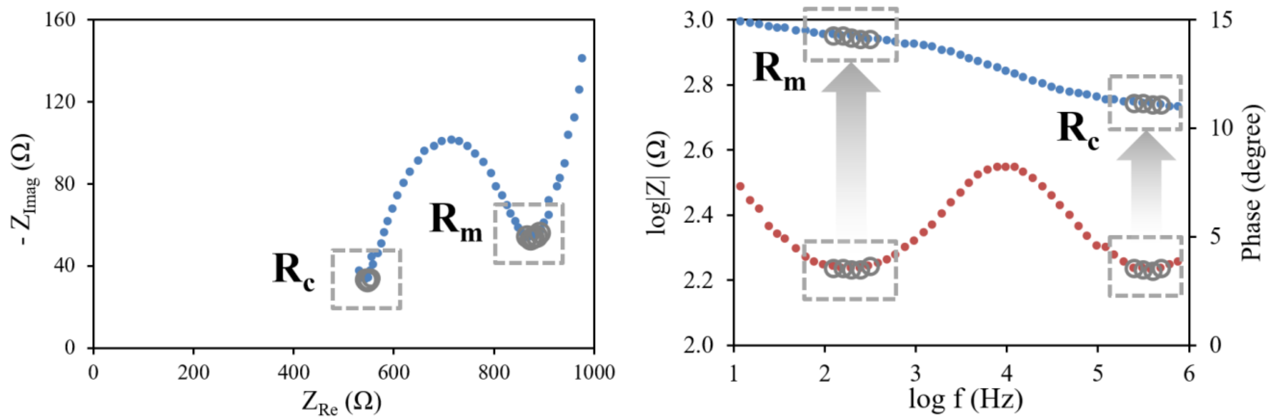

Fig. 15. EIS of mortars reinforced with CF showing the points used for the calculation of R (circled): in the Nyquist plot (left), the two cusps identify the resistance of the matrix R_m (low frequencies) and of the composite R_c (high frequencies). In the Bode plot (right) the circled points of the phase-frequency curve (red points), closest to 0°, represent the two resistive behaviors of the FRCM.

Based on these experimental results for FRCMs, the determination of the specific electrical resistivity of the examined mortars was based on the average values of log |Z| (Eq. 1-2), selected at high frequencies setting a PAT close to zero. In this way, only the composite resistance R_c was considered, considering the combined conductive mechanisms of the cement matrix and conductive fibers (hence the behavior of the FRCMs).

The trends of the electrical resistivity of the mortars during the curing period and the ultimate ρ values (at 91 days) are shown in Figs. 16 and 17, respectively.

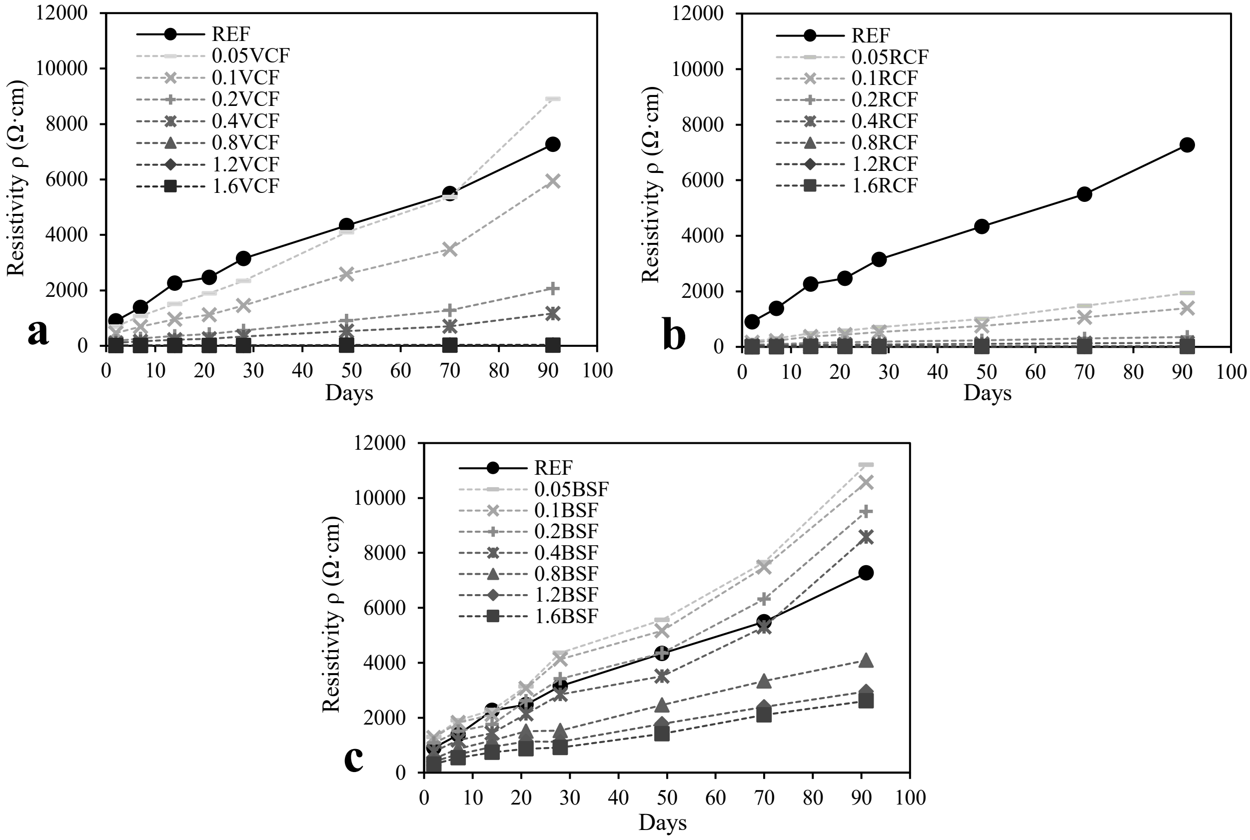

Fig. 16. Trends of electrical resistivity (ρ) during the curing period of mortars reinforced with: VCFs (a), RCFs (b), BSFs (c).

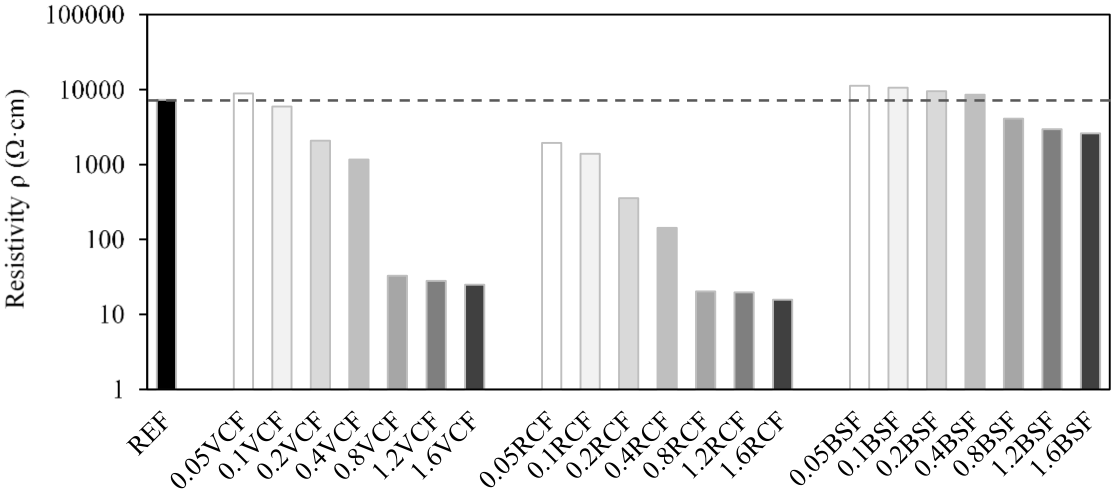

Fig. 17. Electrical resistivity (ρ) after 91 days curing for the mortars reinforced with: VCFs, RCFs and BSFs.

The results clearly show the high ability of CFs to decrease the electrical resistivity of the mortars. All mixtures show a gradual increase of the electrical resistivity during the curing period (Fig. 16) due to gradual water loss. Nevertheless, these increases are very low in CF-reinforced mortars because the electrical conduction between the carbon filaments overpowers the ionic conduction of the solution within the pores. Particularly, RCFs (also at low concentrations) produce a very high decrease in the resistivity in the early stages of curing, and the ρ values remain almost the same during longer test periods (Fig. 16c).

The electrical effectiveness of the addition of CFs is clearly visible in the logarithmic histogram, where the ultimate ρ values of the mixtures are shown (Fig. 17). Mortars with high VCF and RCF contents (≥0.8 vol.%) show resistivity values two orders of magnitude lower than the REF mixture. Even at intermediate concentrations (0.2–0.4 vol.%) the addition of CFs is very effective, since the 0.2 VCF and 0.2 RCF mortars show resistivity values 72% and 95% lower compared to the REF, respectively. Contrariwise, BSFs require high doses to significantly reduce the mortar resistivity, since the 1.6 BSF addition shows a 64% resistivity decrease.

From the results, the so-called "percolation threshold" was assessed: it represents the fiber amount that transforms the cement-based composite from an insulator to a semi-conductor and to a conductor, thanks to a remarkable decrease in electrical resistivity [38]. This is a very important parameter, since it has been demonstrated that several properties of multifunctional cement-based composites, such as stress-sensitivity, are maximized within the percolation zone [77–80]. The relationship between the fiber concentration and electrical resistivity is given in Fig. 18.

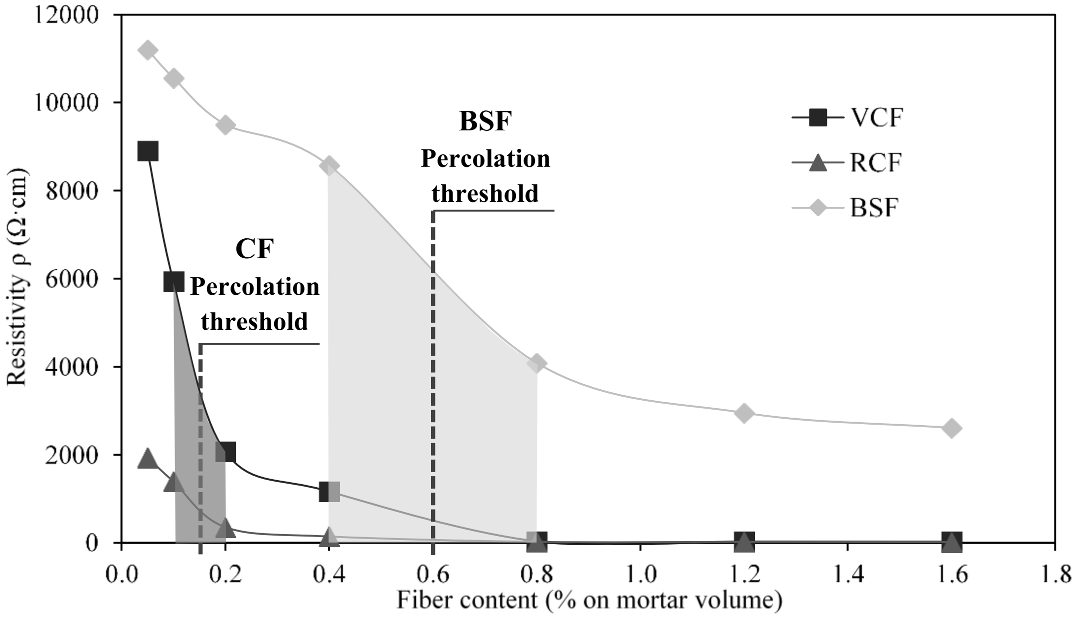

Fig. 18. Ultimate electrical resistivity (ρ) of mortars vs. fibers concentration.

The curves show a remarkable decrease in the electrical resistivity of mortars, with concentrations of VCF and RCF between 0.1 and 0.2 vol.%, which are considered as the extremes of the percolation zone of CFs [81]. In this area, VCFs decrease the resistivity of the mixture from 5941 to 2070 Ω·cm, which corresponds to a decrease of 65%. The effect of RCFs on the electrical properties is more evident, since there is a decrease from 1392 Ω·cm to 355 Ω·cm, by moving from 0.1 RCF to 0.2 RCF concentrations, with an approximate drop of one order of magnitude. On the contrary, the percolation zone of BSFs is placed between 0.4 and 0.8 vol.%, where the ρ ranges from 8573 to 4089 Ω·cm, with a decrease of 52%.

The very high decrease of the electrical resistivity shown by the mortars beyond the percolation threshold is related to the predominance of the electric contacts among the fibers on the ionic conductivity of the cement matrix, owing to its high concentration of fibers [11,82]. This is also demonstrated by the poor influence of water loss on the electrical properties of mortars with high CF content (≥ 0.8 vol.%) during the curing period (Figs. 16a–16b), with resistivity values rising from 6–12 Ω·cm at 2 days, to only 16–33 Ω·cm at 91 days. The most interesting result is the high effectiveness of RCFs on decreasing the electrical resistivity of the mortars, even at low dosages. For example, the 0.05 RCF mortar shows an ultimate ρ of 1934 Ω·cm, which is 73% less than the plain mortar. The high quantity of carbon micro-particles in the RCFs (Fig. 1b) increases their functional electrical surface, thereby creating effective conductive paths, even at low concentrations. The functionality of RCFs at low dosages could lead to a strong incentive for the development of high conductive concretes, thanks to the decrease in costs (the price of RCFs is 66% lower than VCFs, see Table 2) and the greater sustainability. On the other hand, the high electrical resistivity of the BSF-reinforced mortars is linked to both the low electrical properties of the SFs [43] and their lower aspect ratio. As widely demonstrated in the literature [36], fibers with a lower aspect ratio form a less effective conductive network, thereby decreasing their electrical contact bridges. As a consequence, the percolation threshold of BSF mortars is significantly higher than that of CF mortars as Fig. 18 clearly shows.

4. Conclusions

In this study, the effects of different types of electrically conductive fibers were investigated within structural mortars, in terms of their mechanical strength, durability, and electrical properties. 6 mm-long virgin carbon fibers, recycled carbon fibers, and brass-plated steel fibers were added into the mixtures in seven different concentrations, from 0.05% to 1.6%, by mortar volume.

The results of the tests suggest the following conclusions:

- The addition of fibers enhances the flexural and tensile splitting strength of the mortars, thanks to the bridging effect. RCFs show very high mechanical performances by increasing R_f and f_{ct} values up to 201% and 189% compared to the REF, respectively. SEM investigations allow to relate these results to the high presence of carbon micro-fragments on the RCF surface. These fragments increase the roughness of the fibers' surfaces, thereby functioning as nucleation points for C-S-H and, at the same time, they improve the adhesion between the fibres and the cement matrix. The addition of fibers also increases compressive strength, although very high concentrations of CFs lead to slight decreases in R_c, due to the presence of voids produced by fiber clumps. BSFs, thanks to their dimensional characteristics, greatly improve the post-cracking toughness of the composites, with values above 50 MPa, and with an ultimate CMOD of up to 0.72 mm.
- Porosimetric tests prove that the addition of fibers leads to a microstructural refinement of the cement paste, thereby decreasing both the total porosity volume (V_p) and the average pore diameter (d_p). A higher amount of fibers also leads to lower capillary water absorption over a long period, thanks to the lower content of capillary pores by volume within the mortar. Furthermore, all FRMs show lower absorption coefficients (C) than the plain mortar.
- The poor volume of capillary pores also leads to a lower free drying shrinkage of mortars with high-fiber content during the curing period. Mixtures 1.6 RCF and 1.6 BSF achieved the lowest shrinkage strain (ε_s) values, with a decrease of 38% compared to the plain mortar.
- Concerning the multi-phase electrical behavior of mortars, the EIS technique allows a good distinction between electrical resistance of the cement matrix (R_m) and the resistance of the matrix–fiber composite (R_c), detected at low and high frequencies, respectively. High frequency impedances show that the addition of CFs decreases the electrical resistivity of the mortars up to several orders of magnitude compared to the plain mortar. In particular, the RCFs showed very high effectiveness, with noticeable resistivity reductions even in the cases of low fiber dosages. This result is related to the high number of carbon micro-particles, which increase the specific conductive surfaces of RCFs. The percolation threshold is between 0.1 and 0.2 vol.% fiber concentration for the VCFs and RCFs, with decreases of ρ equal to 65% and 75%, respectively. The BSFs show lower electrical effectiveness, with a percolation threshold between 0.4 and 0.8 vol.%, with decreases of ρ equal to 52% compared to the REF.

In light of these results, it can be stated that the addition of conductive fibers not only enhances the electrical properties of cement-based materials, but also their mechanical strength and durability. The study of several concentrations allows estimation of the optimal amount of fibers for the production of multifunctional and high-performance materials with high electrical properties suitable for SHM systems, electromagnetic shielding, and many other fields of study. The study of fiber amounts within concrete for real structural applications will be the most promising topic for future research.

Acknowledgements

The authors wish to thank STW GmbH, Apply Carbon SA, Bekaert SA and BASF SE for carbon fibers, steel fibers and superplasticizer kindly offered for this work.

References

[1] B. Han, X. Yu, J. Ou, Self-Sensing Concrete in Smart Structures, 2014. doi:10.1016/C2013-0-14456-X.
[2] F. Sanchez, K. Sobolev, Nanotechnology in concrete - A review, Constr. Build. Mater. 24 (2010) 2060–2071. doi:10.1016/j.conbuildmat.2010.03.014.
[3] R.M. Andrew, Global CO2 emissions from cement production, Earth Syst. Sci. Data Discuss. 10 (2018) 195–217. doi:10.5194/essd-10-195-2018.
[4] J. Lehne, F. Preston, Making Concrete Change; Innovation in Low-carbon Cement and Concrete, Chatham House Rep. (2018) 1–122. doi:10.1088/1742-6596/1015/3/032163.
[5] L. Coppola, D. Coffetti, E. Crotti, Pre-packed alkali activated cement-free mortars for repair of existing masonry buildings and concrete structures, Constr. Build. Mater. 173 (2018) 111–117. doi:10.1016/j.conbuildmat.2018.04.034.
[6] B. Suryanto, W.J. McCarter, G. Starrs, S.A. Wilson, R.M. Traynor, Smart cement composites for durable and intelligent infrastructure, Procedia Eng. 125 (2015) 796–803. doi:10.1016/j.proeng.2015.11.139.
[7] B. Han, L. Zhang, J. Ou, Smart and Multifunctional Concrete Towards Sustainable Infrastructures, Springer Singapore, 2017.
[8] C. Giosuè, A. Belli, A. Mobili, B. Citterio, F. Biavasco, M.L. Ruello, F. Tittarelli, Improving the impact of commercial paint on indoor air quality by using highly porous fillers, Buildings. 7 (2017). doi:10.3390/buildings7040110.
[9] C. Giosuè, A. Mobili, G. Toscano, M.L. Ruello, F. Tittarelli, Effect of Biomass Waste Materials as Unconventional Aggregates in Multifunctional Mortars for Indoor Application, Procedia Eng. 161 (2016) 655–659. doi:10.1016/j.proeng.2016.08.724.
[10] C. Giosuè, A. Mobili, C. Di Perna, F. Tittarelli, Performance of lightweight cement-based and alkali-activated mortars exposed to high-temperature, Constr. Build. Mater. 220 (2019) 565–576. doi:10.1016/j.conbuildmat.2019.05.193.
[11] B. Han, L. Zhang, C. Zhang, Y. Wang, X. Yu, J. Ou, Reinforcement effect and mechanism of carbon fibers to mechanical and electrically conductive properties of cement-based materials, Constr. Build. Mater. 125 (2016) 479–489. doi:10.1016/j.conbuildmat.2016.08.063.
[12] D.D.L. Chung, Cement reinforced with short carbon fibers: A multifunctional material, Compos. Part B Eng. 31 (2000) 511–526. doi:10.1016/S1359-8368(99)00071-2.
[13] G. Yıldırım, O. Öztürk, A. Al-Dahawi, A. Afşın Ulu, M. Şahmaran, Self-sensing capability of Engineered Cementitious Composites: Effects of aging and loading conditions, Constr. Build. Mater. 231 (2020). doi:10.1016/j.conbuildmat.2019.117132.
[14] G. Yıldırım, M.H. Sarwary, A. Al-Dahawi, O. Öztürk, Ö. Anıl, M. Şahmaran, Piezoresistive behavior of CF- and CNT-based reinforced concrete beams subjected to static flexural loading: Shear failure investigation, Constr. Build. Mater. 168 (2018) 266–279. doi:10.1016/j.conbuildmat.2018.02.124.
[15] A.O. Monteiro, P.B. Cachim, P.M.F.J. Costa, Self-sensing piezoresistive cement composite loaded with carbon black particles, Cem. Concr. Compos. 81 (2017) 59–65. doi:10.1016/j.cemconcomp.2017.04.009.
[16] A. Belli, A. Mobili, T. Bellezze, F. Tittarelli, P.B. Cachim, Piezoresistive behavior of mortars loaded with graphene and carbon fibers for the development of self-sensing composites, in: Taylor & Francis Group (Ed.), Adv. Trends Eng. Sci. Technol. III- Proc. 3rd

Int. Conf. Eng. Sci. Technol. ESaT 2018, 2019: pp. 37–42.

[17] J. Gomis, O. Galao, V. Gomis, E. Zornoza, P. Garcés, Self-heating and deicing conductive cement. Experimental study and modeling, Constr. Build. Mater. 75 (2015) 442–449. doi:10.1016/j.conbuildmat.2014.11.042.

[18] A.O. Monteiro, A. Loredo, P.M.F.J. Costa, M. Oeser, P.B. Cachim, A pressure-sensitive carbon black cement composite for traffic monitoring, Constr. Build. Mater. 154 (2017) 1079–1086. doi:10.1016/j.conbuildmat.2017.08.053.

[19] N. Kaur, S. Bhalla, Combined Energy Harvesting and Structural Health Monitoring Potential of Embedded Piezo-Concrete Vibration Sensors, J. Energy Eng. 141 (2015). doi:10.1061/(ASCE)EY.1943-7897.0000224.

[20] L. Zhang, B. Han, J. Ouyang, X. Yu, S. Sun, J. Ou, Multifunctionality of cement based composite with electrostatic self-assembled CNT/NCB composite filler, Arch. Civ. Mech. Eng. 17 (2017) 354–364. doi:10.1016/j.acme.2016.11.001.

[21] A.L. Materazzi, F. Ubertini, A. D'Alessandro, Carbon nanotube cement-based transducers for dynamic sensing of strain, Cem. Concr. Compos. 37 (2013) 2–11. doi:10.1016/j.cemconcomp.2012.12.013.

[22] J.L. Le, H. Du, S.D. Pang, Use of 2-D Graphene Nanoplatelets (GNP) in cement composites for structural health evaluation, Compos. Part B Eng. 67 (2014) 555–563. doi:10.1016/j.compositesb.2014.08.005.

[23] A.L. Pisello, A. D'Alessandro, S. Sambuco, M. Rallini, F. Ubertini, F. Asdrubali, A.L. Materazzi, F. Cotana, Multipurpose experimental characterization of smart nanocomposite cement-based materials for thermal-energy efficiency and strain-sensing capability, Sol. Energy Mater. Sol. Cells. 161 (2017) 77–88. doi:10.1016/j.solmat.2016.11.030.

[24] A. Belli, A. Mobili, T. Bellezze, F. Tittarelli, P. Cachim, Evaluating the self-sensing ability of cement mortars manufactured with graphene nanoplatelets, virgin or recycled carbon fibers through piezoresistivity tests, Sustain. 10 (2018). doi:10.3390/su10114013.

[25] A.O. Monteiro, P.B. Cachim, P.M.F.J. Costa, Electrical Properties of Cement-based Composites Containing Carbon Black Particles, Mater. Today Proc. 2 (2015) 193–199. doi:10.1016/j.matpr.2015.04.021.

[26] P.W. Chen, D.D.L. Chung, Carbon fiber reinforced concrete for smart structures capable of non-destructive flaw detection, Smart Mater. Struct. 2 (1993) 22–30. doi:10.1088/0964-1726/2/1/004.

[27] D.V. Badami, J.C. Joiner, G.A. Jones, Microstructure of High Strength, High Modulus Carbon Fibres, Nature. 215 (1967) 386–387. doi:10.1038/215386a0.

[28] Y.-P. Jeon, R. Alway-Cooper, M. Morales, A.A. Ogale, Carbon Fibers, Handb. Adv. Ceram. (2013) 143–154. doi:10.1016/B978-0-12-385469-8.00009-5.

[29] H. Nguyen, T. Fujii, K. Okubo, V. Carvelli, Cement mortar reinforced with recycled carbon fiber and CFRP waste, ECCM 2016 - Proceeding 17th Eur. Conf. Compos. Mater. (2016).

[30] M. Mastali, A. Dalvand, The impact resistance and mechanical properties of self-compacting concrete reinforced with recycled CFRP pieces, Compos. Part B Eng. 92 (2016) 360–376. doi:10.1016/j.compositesb.2016.01.046.

[31] Y. Hu, D. Luo, P. Li, Q. Li, G. Sun, Fracture toughness enhancement of cement paste with multi-walled carbon nanotubes, Constr. Build. Mater. 70 (2014) 332–338. doi:10.1016/j.conbuildmat.2014.07.077.

[32] Z. shun Chen, X. Zhou, X. Wang, P. Guo, Mechanical behavior of multilayer GO carbon-fiber cement composites, Constr. Build. Mater. 159 (2018) 205–212. doi:10.1016/j.conbuildmat.2017.10.094.

[33] P.W. Chen, D.D.L. Chung, Low-drying-shrinkage concrete containing carbon fibers, Compos. Part B Eng. 27 (1996) 269–274. doi:10.1016/1359-8368(95)00020-8.

[34] S. Wen, D.D.L. Chung, The role of electronic and ionic conduction in the electrical conductivity of carbon fiber reinforced cement, Carbon N. Y. 44 (2006) 2130–2138.

doi:10.1016/j.carbon.2006.03.013.
[35] C.G. Berrocal, K. Hornbostel, M.R. Geiker, I. Löfgren, K. Lundgren, D.G. Bekas, Electrical resistivity measurements in steel fibre reinforced cementitious materials, Cem. Concr. Compos. 89 (2018) 216–229. doi:10.1016/j.cemconcomp.2018.03.015.
[36] M. Chiarello, R. Zinno, Electrical conductivity of self-monitoring CFRC, Cem. Concr. Compos. 27 (2005) 463–469. doi:10.1016/j.cemconcomp.2004.09.001.
[37] H. Whittington, J. McCarter, M. Forde, The conduction of electricity through concrete, Mag. Concr. Res. 33 (1981) 48–59.
[38] P. Xie, P. Gu, J.J. Beaudoin, Electrical percolation phenomena in cement composites containing conductive fibres, J. Mater. Sci. 31 (1996) 4093–4097. doi:10.1007/BF00352673.
[39] R.M. Chacko, Carbon-Fiber Reinforced Cement Based Sensors, Univ. Br. Columbia, Master Degree Thesis Civ. Eng. (2005). doi:10.14288/1.0063303.
[40] A. Al-Dahawi, O. Öztürk, F. Emami, G. Yildirim, M. Şahmaran, Effect of mixing methods on the electrical properties of cementitious composites incorporating different carbon-based materials, Constr. Build. Mater. 104 (2016) 160–168. doi:10.1016/j.conbuildmat.2015.12.072.
[41] J. Donnini, T. Bellezze, V. Corinaldesi, Mechanical, electrical and self-sensing properties of cementitious mortars containing short carbon fibers, J. Build. Eng. 20 (2018) 8–14. doi:10.1016/j.jobe.2018.06.011.
[42] Q. Liu, Q. Xu, Q. Yu, R. Gao, T. Tong, Experimental investigation on mechanical and piezoresistive properties of cementitious materials containing graphene and graphene oxide nanoplatelets, Constr. Build. Mater. 127 (2016) 565–576. doi:10.1016/j.conbuildmat.2016.10.024.
[43] N. Banthia, S. Djeridane, M. Pigeon, Electrical resistivity of carbon and steel micro-fiber reinforced cements, Cem. Concr. Res. 22 (1992) 804–814. doi:10.1016/0008-8846(92)90104-4.
[44] L. Fiala, J. Toman, J. Vodička, V. Ráček, Experimental Study on Electrical Properties of Steel-fibre Reinforced Concrete, Procedia Eng. 151 (2016) 241–248. doi:10.1016/j.proeng.2016.07.362.
[45] A. Mazzoli, V. Corinaldesi, J. Donnini, C. Di Perna, D. Micheli, A. Vricella, R. Pastore, L. Bastianelli, F. Moglie, V. Mariani Primiani, Effect of graphene oxide and metallic fibers on the electromagnetic shielding effect of engineered cementitious composites, J. Build. Eng. 18 (2018) 33–39. doi:10.1016/j.jobe.2018.02.019.
[46] S. Erdem, S. Hanbay, M.A. Blankson, Self-sensing damage assessment and image-based surface crack quantification of carbon nanofibre reinforced concrete, Constr. Build. Mater. 134 (2017) 520–529. doi:10.1016/j.conbuildmat.2016.12.197.
[47] H. Nguyen, V. Carvelli, T. Fujii, K. Okubo, Cement mortar reinforced with reclaimed carbon fibres, CFRP waste or prepreg carbon waste, Constr. Build. Mater. 126 (2016) 321–331. doi:10.1016/j.conbuildmat.2016.09.044.
[48] F. Tittarelli, Effect of low dosages of waste GRP dust on fresh and hardened properties of mortars: Part 2, Constr. Build. Mater. 47 (2013) 1539–1543. doi:10.1016/j.conbuildmat.2013.06.086.
[49] F. Tittarelli, A. Mobili, C. Giosuè, A. Belli, T. Bellezze, Corrosion behaviour of bare and galvanized steel in geopolymer and Ordinary Portland Cement based mortars with the same strength class exposed to chlorides, Corros. Sci. 134 (2018). doi:10.1016/j.corsci.2018.02.014.
[50] V.A. Rossetti, Concrete: Materials and Technology, McGraw-Hill, 2007.
[51] M. Collepardi, Durability of concrete: theory, practice and specification requirements - Part I: causes of chemical degradation, Ital. Cem. Ind. 671 (1992) 1992.
[52] A. Mobili, A. Belli, C. Giosuè, T. Bellezze, F. Tittarelli, Metakaolin and fly ash alkali-activated mortars compared with cementitious mortars at the same strength class, Cem.

Concr. Res. 88 (2016) 198–210. doi:10.1016/j.cemconres.2016.07.004.
[53] B. Han, X. Guan, J. Ou, Electrode design, measuring method and data acquisition system of carbon fiber cement paste piezoresistive sensors, Sensors Actuators, A Phys. 135 (2007) 360–369. doi:10.1016/j.sna.2006.08.003.
[54] M. Sahmaran, G. Yıldırım, G. Aras, S. Keskin, O. Keskin, M. Lachemi, Self healing of cementitious composites to reduce high CO2 emissions, Mater. J. 114 (2017) 93–104. doi:10.1111/j.1469-7610.2010.02280.x.
[55] C. Pierini, Steel Fibers Reinforced Concrete (SFRC), Characterization of the material and structural design, Ingenio. 41 (2016) 46.
[56] D. Yoo, S. Kim, G. Park, J. Park, S. Kim, Effects of fiber shape , aspect ratio , and volume fraction on flexural behavior of ultra-high-performance fiber-reinforced cement composites, Compos. Struct. 174 (2017) 375–388. doi:10.1016/j.compstruct.2017.04.069.
[57] R. Hameed, A. Turatsinze, F. Duprat, A. Sellier, Metallic fiber reinforced concrete: Effect of fiber aspect ratio on the flexural properties, ARPN J. Eng. Appl. Sci. 4 (2009) 67–72.
[58] K. Ogi, T. Shinoda, M. Mizui, Strength in concrete reinforced with recycled CFRP pieces, Compos. Part A Appl. Sci. Manuf. 36 (2005) 893–902. doi:10.1016/j.compositesa.2004.12.009.
[59] M. Mastali, A. Dalvand, A. Sattarifard, The impact resistance and mechanical properties of the reinforced self-compacting concrete incorporating recycled CFRP fiber with different lengths and dosages, Compos. Part B Eng. 112 (2017) 74–92. doi:10.1016/j.compositesb.2016.12.029.
[60] L. Vandewalle, Postcracking Behaviour of Hybrid Steel Fiber Reinforced Concrete, 6th Int. Conf. Fract. Mech. Concr. Concr. Struct. (2007) 17–22.
[61] B. Wang, Y. Zhang, H. Ma, Porosity and pore size distribution measurement of cement/carbon nanofiber composites by 1H low field nuclear magnetic resonance, J. Wuhan Univ. Technol. Mater. Sci. Ed. 29 (2014) 82–88. doi:10.1007/s11595-014-0871-1.
[62] M. Collepardi, The New Concrete, (2010).
[63] G.M. Kim, H.N. Yoon, H.K. Lee, Autogenous shrinkage and electrical characteristics of cement pastes and mortars with carbon nanotube and carbon fiber, Constr. Build. Mater. 177 (2018) 428–435. doi:10.1016/j.conbuildmat.2018.05.127.
[64] J. Rhodes, D. Carreira, J. Beaudoin, B. Gamble, H. Geymayer, B. Goyal, B. Hope, J. Keeton, C. Kesler, ACI 209R-92, Prediction of Creep, Shrinkage, and Temperature Effects in Concrete Structures, Rep. by ACI Comm. 209. 29 (2000) 143–148. doi:10.1080/03064220008536699.
[65] A. Mobili, C. Giosuè, A. Belli, T. Bellezze, F. Tittarelli, Geopolymeric and cementitious mortars with the same mechanical strength class: Performances and corrosion behaviour of black and galvanized steel bars, in: Am. Concr. Institute, ACI Spec. Publ., 2015.
[66] W. McCarter, S. Garvin, N. Bouzid, Impedance measurements on cement paste, J. Mater. Sci. Lett. 7 (1988) 1056–1057. doi:10.1007/ BF00720825.
[67] W.J. McCarter, R. Brousseau, The A.C. response of hardened cement paste, Cem. Concr. Res. 20 (1990) 891–900. doi:10.1016/0008- 8846(90)90051-X.
[68] P. Gu, Z. Xu, P. Xie, J. Beaudoin, Application of A.C. impedance techniques in studies of porous cementitious materials, Cem. Concr. Res. 23 (1993) 531–540. doi:10.1016/0008-8846(93)90003-R.
[69] C. Scuderi, T. Mason, H. Jennings, Impedance spectra of hydrating cement pastes, J. Mater. Sci. 26. 26 (1991) 349.353. doi:10.1007/ BF00576526.
[70] S. Ford, J. Shane, T. Mason, Assignment of features in impedance spectra of the cement-paste/steel system, Cem. Concr. Res. 28 (1998) 1737–1751. doi:10.1016/S0008-8846(98)00156-2.
[71] R. Coverdale, B. Christensen, H. Jennings, T. Mason, D. Bentz, E. Garboczi, Interpretation of impedance spectroscopy of cement paste via computer modelling, J. Mater. Sci. 30 (1995)

712–719. doi:10.1007/BF00356331.
[72] J.M. Torrents, T.O. Mason, E.J. Garboczi, Impedance spectra of fiber-reinforced cement-based composites: A modeling approach, Cem. Concr. Res. 30 (2000) 585–592. doi:10.1016/S0008-8846(00)00211-8.
[73] J. Torrents, T. Mason, A. Peled, S. Shah, E. Garboczi, Analysis of the impedance spectra of short conductive fiber-reinforced composites, J. Mater. Sci. 36. 36 (2001) 4003–4012.
[74] A. Hixson, L. Woo, M. Campo, T. Mason, E. Garboczi, Intrinsic conductivity of short conductive fibers in composites by impedance spectroscopy, J. Electroceram. 7 (2001) 189–195.
[75] T.O. Mason, M.A. Campo, A.D. Hixson, L.Y. Woo, Impedance spectroscopy of fiber-reinforced cement composites, Cem. Concr. Compos. 24 (2002) 457–465. doi:10.1016/S0958-9465(01)00077-4.
[76] A.D. Hixson, L.Y. Woo, M.A. Campo, T.O. Mason, The origin of nonlinear currentevoltage behavior in fiber-reinforced cement composites, Cem. Concr. Res. 33. 33 (2003) 835–840. doi:10.1016/S0008-8846(02) 01062-1.
[77] H. Li, H. gang Xiao, J. ping Ou, Effect of compressive strain on electrical resistivity of carbon black-filled cement-based composites, Cem. Concr. Compos. 28 (2006) 824–828. doi:10.1016/j.cemconcomp.2006.05.004.
[78] B.G. Han, B.Z. Han, X. Yu, Effects of the content level and particle size of nickel powder on the piezoresistivity of cement-based composites/sensors, Smart Mater. Struct. 19 (2010). doi:doi:10.1088/0964-1726/19/6/065012.
[79] S. Mohamed, Wireless and embedded carbon nanotube networks for damage detection in concrete structures, Nanotechnology. 20 (2009). doi:10.1088/0957-4484/20/39/395502.
[80] A. Al-Dahawi, M.H. Sarwary, O. Öztürk, G. Yildirim, A. Akin, M. Şahmaran, M. Lachemi, Electrical percolation threshold of cementitious composites possessing self-sensing functionality incorporating different carbon-based materials, Smart Mater. Struct. 25 (2016). doi:10.1088/0964-1726/25/10/105005.
[81] B. Han, S. Ding, X. Yu, Intrinsic self-sensing concrete and structures: A review, Meas. J. Int. Meas. Confed. 59 (2015) 110–128. doi:10.1016/j.measurement.2014.09.048.
[82] R. Zallen, Physics of Amorphous Solids, Wiley, New York. (1983) 135–204.